Disordered zinc in Zn_4Sb_3 with phonon-glass and electron-crystal thermoelectric properties

G. JEFFREY SNYDER[1,2]*, MOGENS CHRISTENSEN[3], EIJI NISHIBORI[4], THIERRY CAILLAT[2] AND BO BRUMMERSTEDT IVERSEN[3]

[1]California Institute of Technology, Materials Science, 1200 East California Boulevard, Pasadena, California 91125, USA
[2]Jet Propulsion Laboratory/California Institute of Technology, 4800 Oak Grove Drive, Pasadena, California 91109, USA
[3]Department of Chemistry, University of Aarhus, DK-8000 Aarhus, Denmark
[4]Department of Applied Physics, Nagoya University, Nagoya 464-8603, Japan
*e-mail: jsnyder@caltech.edu

Published online: 27 June 2004; doi:10.1038/nmat1154

By converting waste heat into electricity, thermoelectric generators could be an important part of the solution to today's energy challenges. The compound Zn_4Sb_3 is one of the most efficient thermoelectric materials known. Its high efficiency results from an extraordinarily low thermal conductivity in conjunction with the electronic structure of a heavily doped semiconductor. Previous structural studies have been unable to explain this unusual combination of properties. Here, we show through a comprehensive structural analysis using single-crystal X-ray and powder-synchrotron-radiation diffraction methods, that both the electronic and thermal properties of Zn_4Sb_3 can be understood in terms of unique structural features that have been previously overlooked. The identification of Sb^{3-} ions and Sb_2^{4-} dimers reveals that Zn_4Sb_3 is a valence semiconductor with the ideal stoichiometry $Zn_{13}Sb_{10}$. In addition, the structure contains significant disorder, with zinc atoms distributed over multiple positions. The discovery of glass-like interstitial sites uncovers a highly effective mechanism for reducing thermal conductivity. Thus Zn_4Sb_3 is in many ways an ideal 'phonon glass, electron crystal' thermoelectric material.

The efficiency of a thermoelectric generator depends on the thermoelectric figure of merit zT, where z is defined as $z = \alpha^2\sigma/\kappa$, ($\alpha$ is the Seebeck coefficient, σ is the electrical conductivity, T is temperature and κ is the thermal conductivity). Good thermoelectric materials are typically heavily doped semiconductors with low thermal conductivity. Heavily doped semiconductors provide a balance between the large $|\alpha|$ of lightly doped semiconductors and the high σ of metals. The power factor $\alpha^2\sigma$ in Zn_4Sb_3 (13 $\mu W\,cm^{-1}\,K^{-2}$ at 400 °C)[1] is reasonably high, but still less than half that of the next best thermoelectric material—$(AgSbTe_2)_{0.15}(GeTe)_{0.85}$ (TAGS) (ref. 2). What makes Zn_4Sb_3 a remarkable thermoelectric material is the unusually low thermal conductivity (Fig. 1), comparable to that of a glass.

The total thermal conductivity is the sum of the lattice thermal conductivity and the electronic thermal conductivity, where the latter can be estimated from the electrical conductivity using the Wiedemann–Franz law. The lattice thermal conductivity usually can be understood from the features of the crystal structure. Complex structures with large unit cells, disorder, and/or a variety of atom types are known to scatter phonons and therefore produce materials with low thermal conductivities. For example, binary skutterudites such as $CoSb_3$ can have a high power factor, but they require disorder, electron–phonon scattering, or introduction of rattling guest atoms to lower the lattice thermal conductivity enough to achieve high zT values[3,4]. Glasses have even lower thermal conductivity compared with crystalline materials because the amorphous structure scatters phonons to mean-free paths of atomic dimensions. An amorphous structure will also scatter electrons, lowering their mobility and therefore electrical conductivity and power factor. Thus the ideal thermoelectric material resembles a 'phonon glass and an electron crystal'[5,6].

Virtually all thermoelectric materials with the highest zT are compound semiconductors containing heavy elements. In such materials, the general electronic properties can be explained from their crystal structures by identifying and locating atoms and their covalent and ionic bonds. Bonding strong enough to produce a small bandgap is required for semiconducting electronic properties, which allows the possibility of high Seebeck coefficient.

Thus, a proper description of the crystal structure of Zn_4Sb_3 should explain both the electronic structure (by identifying bonds and

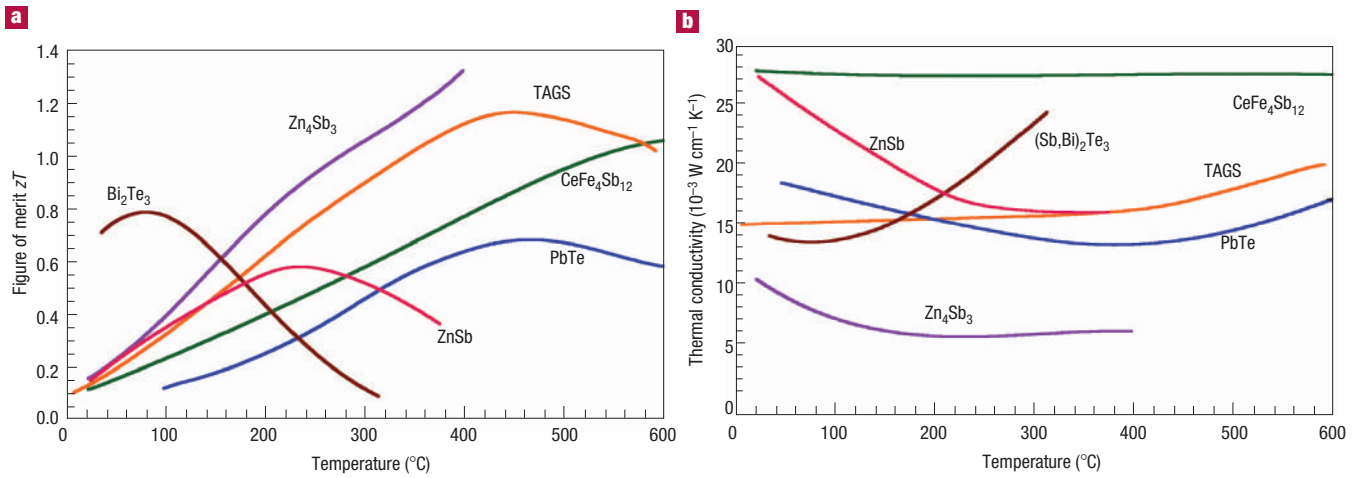

Figure 1 Thermoelectric properties of Zn_4Sb_3 compared with other materials. a, Thermoelectric figure of merit: Zn_4Sb_3 has the highest zT between 150 °C and 400 °C, due to **b**, its thermal conductivity being substantially lower than all other optimized p-type thermoelectric materials[1,2,4,15,17].

therefore valence state) as well as the glass-like thermal conductivity (by identifying phonon-scattering mechanisms) and therefore explain the high thermoelectric figure of merit. The single-crystal X-ray diffraction study of Mayer[7] provides a reasonable starting model of the observed diffraction data, but is inconsistent with numerous chemical and physical properties. The crystal structure reported in the present study allows a general explanation of the electronic transport properties and, in addition, the structure reveals disordered zinc atoms, which explains the remarkable thermoelectric figure of merit.

Both single-crystal and powder X-ray diffraction data were used to determine the detailed crystal structure of Zn_4Sb_3 at room temperature. Small single crystals were extracted from a polycrystalline sample cooled from the melt[8]. Powder samples were synthesised by direct reaction of the elements. The mass density was measured by the immersion method (in toluene) to be 6.36 g cm^{-3}. The initial 14,773 integrated reflections on a small single crystal were reduced to 956 independent reflections (details of the data collection are given in Table S1 of the Supplementary Information), and an empirical absorption correction was carried out on the basis of the large redundancy of the data set. High-resolution synchrotron powder-diffraction data (Supplementary Information, Fig. S2) collected at short wavelength in a thin capillary were used for maximum entropy method (MEM) calculations[9]. The MEM procedure uses scaled, phased, structure factors extracted from the diffraction data by full-pattern Rietveld refinement for finding the most probable electron density consistent with the experimental data.

Table 1 Comparison of structural models for Zn_4Sb_3 with intermediate steps to the interstitial model. The *R* value and goodness-of-fit (GooF) (using the new data set) is improved with each evolution of the model, but the density and composition is close to the experimental values only with the inclusion of interstitials.

	Site occupancy (fraction)				R_F (%)	GooF	x in Zn_xSb_3	Density (g cm^{-3})
Site multiplicity	Zn(1) (36f)	Sb(1) (18e)	Sb(2) (12c)	Zn interstitial (36f)				
Mayer model[7]	1	0.89Sb 0.11Zn	1	0	4.27	2.64	4.07	6.09
Full occupancy model	1	1	1	0	3.93	2.44	3.60	6.21
Vacancy model	0.90	1	1	0	3.45	2.01	3.24	5.96
Three interstitial model	0.90	1	1	0.17	2.57	1.37	3.83	6.37
Empirical values[10,11]							3.95 ± 0.05	6.36

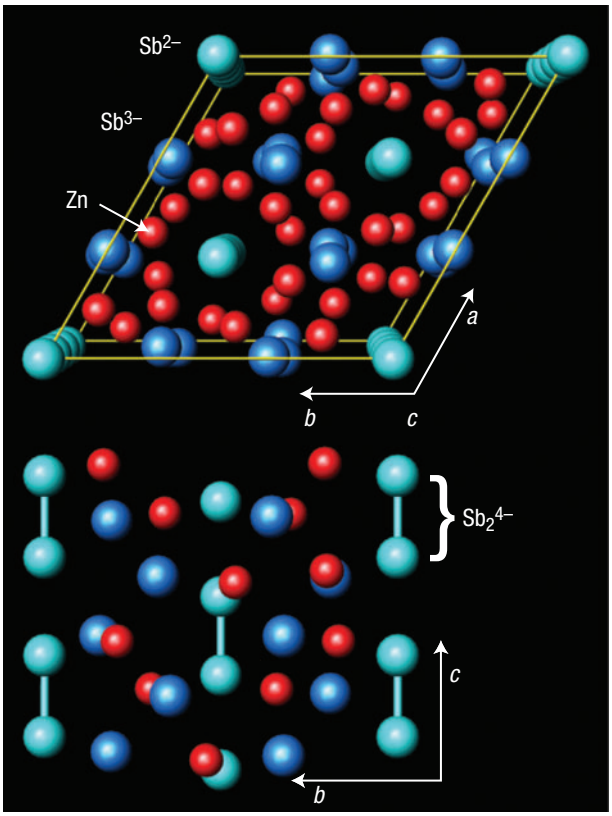

Figure 2 The crystal structure of Zn_4Sb_3 without Zn interstitials. The Sb^{3-} form distorted hexagonal-close-packed layers with Sb^{2-} dimers in the channels formed by the octahedral holes. Top: view along *c*, Bottom: side view showing Sb^{2-} dimers.

Table 2 Atomic coordinates and equivalent isotropic displacement parameters (U_{eq} ($Å^2 \times 10^3$)) for single-crystal refinement of Zn_4Sb_3 ($R\bar{3}c$, a = 12.2282(3) Å, c = 12.4067(4) Å). Standard deviations are given in parentheses.

Atom Site	*x*	*y*	*z*	Occupancy	U_{eq}
Zn(1) 36(f)	0.0792(1)	0.2439(1)	0.4033(1)	0.899(5)	25(1)
Sb(1) 18(e)	0.3555(1)	0	0.25	1	17(1)
Sb(2) 12(c)	0	0	0.1364(1)	1	16(1)
Zn(2) 36(f)	0.1574(14)	0.4207(17)	0.0715(17)	0.046(3)	57(6)
Zn(3) 36(f)	0.2420(20)	0.4600(20)	0.2000(40)	0.056(6)	110(20)
Zn(4) 36(f)	0.1260(20)	0.2367(17)	0.2760(40)	0.063(5)	170(20)

The core structure of Zn_4Sb_3 (Fig. 2), common to all structure solutions[7,10], contains three distinct atom positions (36 Zn(1), 18 Sb(1), and 12 Sb(2)) in space group $R\bar{3}c$ (Table 1, 2). Previous structural investigations have modelled the Sb(1) site with a mixture of Zn (6.7% ref. 10, or 11% ref. 7) and Sb. The substitution of Zn on the Sb(1) site was originally done[11] to achieve the experimental stoichiometry for Zn_xSb_3 known to be $x = 3.95 \pm 0.05$; without any substitution the X-ray stoichiometry would only be $x = 3.6$.

In all our structure determinations, however, we find no evidence of Zn substitution on the Sb(1) site (Table 1). In contrast, all our structure refinements show a deficiency of Zn on the Zn(1) site such that it is only about 90% occupied (corresponding to $x = 3.24$). Clearly, these three atom positions are insufficient to account for the observed Zn stoichiometry.

The MEM electron density (Fig. 3), which is not biased by any particular structural model, shows non-spherical zinc atoms and clearly contains at least three small but unequivocal regions of electron density, separate from the three main atomic positions. If we assign this additional electron density in Zn_4Sb_3 to interstitial Zn atoms, the structural, chemical and physical model of Zn_4Sb_3 is vastly improved. By adding three interstitial sites (Table 2), the *R* value drops dramatically (Table 1) from 4.3% to 2.6% and the goodness-of-fit from 2.6 to 1.4.

To demonstrate the effect of changing the structural model, some intermediate steps are included in Table 1. Starting with the model of Mayer[7], the substitution of Zn on the Sb(1) position is eliminated, then vacancy on the Zn(1) site is allowed, and finally Zn interstitials are added on the basis of the extra electron density found in the MEM density map. Each step significantly improves the *R* value and goodness-of-fit but only the model with Zn-interstitials has low *R* with both stoichiometry and density consistent with experimental observations.

The mass density and stoichiometry of the new structure determination agrees well with the observed density and elemental analysis. The previous structures[7,10] that contain no interstitial atoms and substitute light zinc atoms for heavier antimony are significantly less dense than that observed experimentally (Table 1). This would be quite exceptional because X-ray densities are almost universally slightly greater than experimental densities, due to random vacancies. The density of the revised structure is not only much closer to the observed density (Table 1), but even slightly greater, as expected.

In addition, such a substitution of Zn for Sb leads to conclusions inconsistent with the physical properties. Normally, different elements randomly positioned on the same crystallographic site have the same or very similar size and charge (if the charges differ, then there needs to be some charge compensation elsewhere) and therefore similar site energies. With little energy preference of one element over the other, a range of relative composition for that site should be possible. An example would be an intermetallic alloy of two similar sized, neutral (similar electronegativity) metals that is capable of having a wide range of compositions. However, Zn_4Sb_3 shows none of these properties, it is known to be nearly a line compound with a narrow range of Zn/Sb stoichiometry[11]. Furthermore, the small and electropositive Zn is chemically very different to the large, electronegative Sb. Band-structure calculations[12] show that the Sb(1) site has a coordination sphere with bond distances too large for Zn. The chemical differences between Zn and Sb are made even more apparent by using the concepts of valence compounds.

Valence compounds such as compound semiconductors and Zintl phases are intermediate between insulating and intermetallic compounds. Compound semiconductors are valence compounds containing only covalent bonds whereas Zintl phases contain some ionic bonding[13]. Regardless of the classification, the rules of valence (valence charge balance and the octet rule) stipulate the extent of covalent bonding between anions in analogy to lighter elements of the same family. Like nitrogen, antimony will have formally a –3 valence without any Sb–Sb bonding, –2 valence with one bond, –1 with two bonds and so on. The Sb–Sb bonding can be identified in structures from their distances, which are typically 2.9 ± 0.1 Å; distances greater than 3.3 Å signify significantly weaker bonding[14]. As a consequence of their bonding configurations, valence compounds are usually brittle,

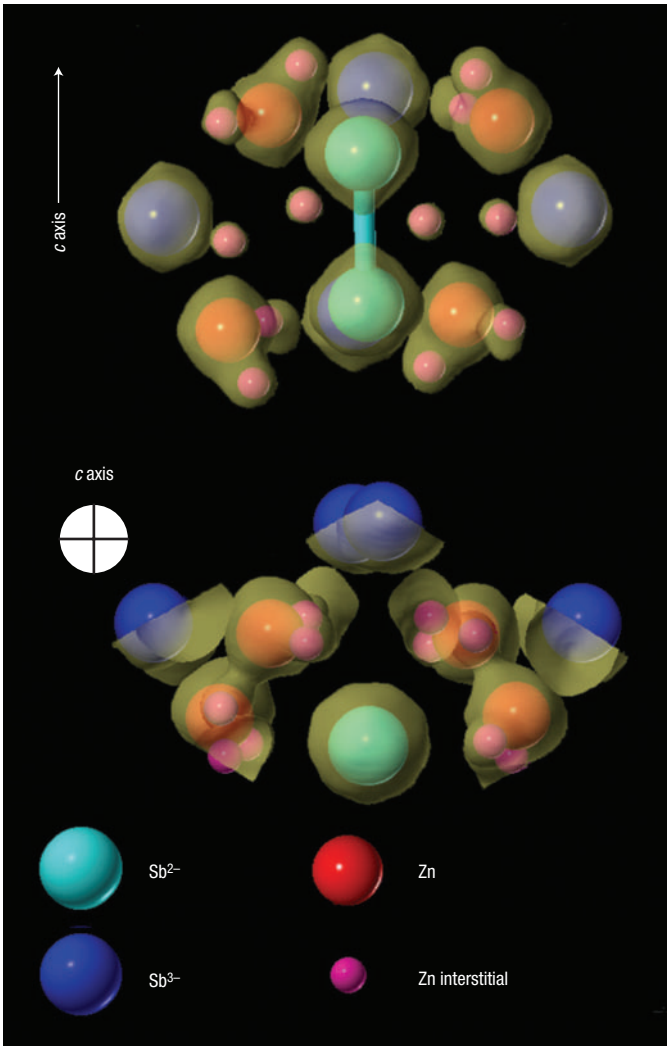

Figure 3 Electron density surface (calculated by MEM) of Zn_4Sb_3 superimposed with the resultant atom positions including three different Zn interstitials.

Table 3 Anisotropic displacement parameters (Å² × 10³) for the single-crystal refinement.

Atom	U_{11}	U_{22}	U_{33}	U_{23}	U_{13}	U_{12}
Sb(1)	19(1)	14(1)	15(1)	–1(1)	0(1)	7(1)
Sb(2)	18(1)	18(1)	12(1)	0	0	9(1)
Zn(1)	26(1)	22(1)	29(1)	1(1)	3(1)	14(1)
Zn(2)	20(6)	56(11)	81(13)	15(9)	–9(6)	8(6)
Zn(3)	57(11)	42(11)	200(40)	–64(18)	63(17)	2(8)
Zn(4)	68(13)	49(10)	400(60)	20(17)	–50(20)	35(10)

diamagnetic semiconductors that, like salts, tolerate little stoichiometric variation of anion/cation ratio. In contrast, intermetallic alloys typically are ductile metals (with low Seebeck coefficient) that can usually tolerate larger stoichiometric variation. The bonding (ionic and covalent) of Sb compounds is typically weaker than that for the lighter elements but enough to produce a small bandgap (required for predominance of n- or p-type carriers) and hence semiconducting electronic properties, namely the possibility of high Seebeck coefficient.

Indeed, most good thermoelectric materials follow the rules of valence compounds. The best-known thermoelectric materials[15] are Bi_2Te_3, Sb_2Te_3 and PbTe, all of which have valence balance, and are small-bandgap semiconductors with limited stoichiometry range. Caesium bismuth telluride $CsBi_4Te_6$ is a good thermoelectric material below room temperature[16], where close examination of the structure reveals that Bi–Bi bonding compensates for the added electron from caesium providing valence balance. The good high-temperature thermoelectric material skutterudite $CoSb_3$ and filled skutterudite (for example, $CeFe_4Sb_{12}$) contains doubly bonded square rings of Sb^- making $(Sb_4)^{4-}$ clusters[3]. Semiconducting $CoSb_3$ (Co^{3+}) has valence balance whereas $CeFe_4Sb_{12}$ (Ce^{3+}, Fe^{2+}) is one electron short of valence balance and therefore a heavily doped p-type semiconductor.

In the Zn–Sb system, the valence compound ZnSb contains singly bonded Sb^{2-}, which form $(Sb_2)^{4-}$ dimers. The assignment of the zinc as Zn^{2+} is consistent with the physical properties (brittle, diamagnetic semiconductor) and with the results of doping additions (substituting Ag^+ for Zn^{2+} produces p-type ZnSb while In^{3+} makes n-type ZnSb)[17].

With the new structure determination, Zn_4Sb_3 is found to follow the rules of valence compounds. The Sb(1) atoms, in a distorted hexagonal-close-packing arrangement, have only zinc near neighbours (6 Zn(1) at 2.76(3) Å; see Table S2 in the Supplementary Information for interatomic distances) and therefore is given the valence designation Sb^{3-}. The Sb(2) atoms are 2.82 Å from another Sb(2) (in addition to 3 Zn(1) at 2.68 Å) indicating the presence of single-bonded Sb^{2-} in dimers similar to those in ZnSb. The Sb^{2-} atoms, like the Al atoms in corundum (Al_2O_3), are in the channels of octahedral holes formed by the Sb^{3-} layers with one dimer every three layers. Zn(1), with four Sb neighbours and one Zn at a metallic distance of 2.7 Å, has two electrons available for covalent or ionic bonding resulting in valence Zn^{2+}. In each hexagonal cell of Zn_4Sb_3, there are 18 Sb^{3-} and 12 Sb^{2-} in dimers requiring a total of 78 electrons, or 39 Zn^{2+} for valence balance ($Zn_{3.9}Sb_3$). As there are only 36 available positions on the main Zn(1) site ($Zn_{3.6}Sb_3$), there must be at least three interstitial zinc atoms for valence balance. The new structure accounts for the interstitial zinc with a total of 38.3(4) Zn atoms per cell ($Zn_{3.83(4)}Sb_3$). The rules of valence should be used to justify chemically the necessity of interstitial zinc, but are not exactly quantitative because complete electron transfer is never expected. Also, because Zn_4Sb_3 is a p-type conductor, it is expected that the composition would be slightly cation-poor (10^{20} holes per $cm^3 = 0.16$ holes per cell = $Zn_{3.89}Sb_3$).

This classification of Zn_4Sb_3 as a valence compound finally gives a general explanation of the chemical and physical properties important to thermoelectric applications. The valence-balance requirement precludes a fixed stoichiometry in both the pure and doped phases. Pure Zn_4Sb_3 is limited to $Zn_{3.95(5)}Sb_3$ whereas doped Zn_4Sb_3 tends to form compensated phases. For example, several percent Ga^{3+} will substitute for Zn^{2+} to make $Ga_{0.16}Zn_{3.66}Sb_3$ but more than one zinc atom is displaced for each gallium atom, such that the resulting compound is nearly isoelectronic, with similar properties, to Zn_4Sb_3. The valence balance also accounts for the relatively large Seebeck coefficient of a small-bandgap semiconductor, essential to an efficient thermoelectric material. The crystal structure used for band-structure calculations[12] to explain the thermoelectric properties of Zn_4Sb_3 is actually closer to the interstitial model than that of Mayer[7]. For these calculations, full occupancy was assumed on the three core positions and extra electrons added to achieve the empirical stoichiometry of Zn.

The three zinc interstitial positions are much like the Zn(1) site, with reasonable distances (>2.5 Å) to three to five neighbouring Sb atoms. Many Zn(1) and Zn-interstitial sites are too close (<2.5 Å) in proximity to be simultaneously occupied, and therefore the site occupancies must be locally correlated. Such correlated disorder will lead to small displacements on neighbouring atoms visible as non-spherical perturbations in the electron density. Thus the actual local coordination of the interstitial atoms will be quite different from that implied from the diffraction data.

The three Zn interstitial sites described here, and perhaps other smaller ones in Zn_4Sb_3, approximate contiguous channels (along the *c* axis), which suggests that there may exist significant Zn mobility in Zn_4Sb_3. The interstitial sites refine best with relatively large, anisotropic thermal parameters where the long axis is in the direction of the closest interstitial or Zn(1) atom (Supplementary Information, Fig. S1). Large, non-ellipsoidal and low-occupancy atom positions are rare in simple inorganic crystals, but are common in intercalation compounds and fast ion-conducting solids[18]. For example, the fast Ag^+ ion conductor α-$RbAg_4I_5$ contains channels of electron density or Ag-interstitial sites. The disorder in Zn_4Sb_3 may be either static or dynamic; indeed, a static-to-dynamic transition may be the origin of the various subtle phase transitions observed[11,19].

The new structure determination reveals disordered interstitials as an extremely effective mechanism for low thermal conductivity that makes Zn_4Sb_3 the highest *zT* thermoelectric in the 150–400 °C temperature range. The compounds ZnSb and Zn_4Sb_3 have very similar structural features and electronic properties[17,20]. However, Zn_4Sb_3 has a much lower thermal conductivity (Fig. 1) than ZnSb, which can be attributed to their most striking difference—interstitial, disordered zinc with large displacement parameters. Some intercalated Chevrel compounds[21] such as $Cu_{4-x}Mo_6S_8$ have similar disordered Cu positions with large thermal-displacement parameters. These phases have promising thermoelectric properties[22], but have not yet demonstrated a thermoelectric figure of merit as large as that of Zn_4Sb_3. The thermal conductivity of Zn_4Sb_3 is substantially lower (Fig. 1) than even filled skutterudite ($CeFe_4Sb_{12}$), which contains a single disordered, 'rattling' site with large displacement parameter[6]. Thus, the multiple, disordered interstitial sites in Zn_4Sb_3 are noticeably more effective at lowering thermal conductivity than even the rattling atom in filled skutterudites.

The thermal conductivity of Zn_4Sb_3 is so low it may be considered a phonon glass. The heat transport of crystalline solids can be successfully modelled using phonons to describe the lattice vibrations. However, for amorphous solids, the phonon mean-free path is of the order of the phonon wavelength, and therefore the lattice vibrations are best described by localized damped oscillators instead of phonons. The resulting thermal conductivity for an amorphous solid is much less than that for a crystalline solid. For real materials, the theoretical thermal conductivity of an amorphous solid can be considered a lower limit to the thermal conductivity[23]. For this reason, it has been suggested that the ideal thermoelectric material is amorphous to phonons while maintaining high electron mobility, the so-called electron crystal phonon glass[5]. It seems that Zn_4Sb_3 is exactly such a compound. The diffuse, disordered channels of zinc seem to reduce the phonon mean-free path substantially. At the same time, the structure of antimony provides a crystalline electronic structure suitable for thermoelectrics.

METHODS

SINGLE-CRYSTAL SAMPLE PREPARATION

Small single crystals were extracted from a polycrystalline sample prepared using the Bridgman technique[8]. Zinc (99.9999%) and antimony (99.999%) shots were combined in a 57.5:42.5 atomic ratio and loaded into a carbon-coated silica ampoule with pointed bottom. The ampoule was evacuated and sealed before placing in a vertical two-zone furnace. The sample was directionally cooled from the melt with a gradient of 50 K cm^{-1} and growth rate of 0.7 K h^{-1}. From power X-ray diffraction and microprobe analysis, the samples seemed to be single phase. Samples often contained microcracks due to phase transformation or instability near the melting point.

SINGLE-CRYSTAL X-RAY DIFFRACTION

Single-crystal (0.1 mm diameter) X-ray diffraction measurements were carried out on a Bruker SMART CCD diffractometer (MoK_α radiation). The single crystals had severe twinning problems, and more than 15 specimens were tested before a suitable sample was found (powder data, unaffected by twinning, give the same results—see below). For the final non-twinned specimen, extensive data were recorded (14,773 integrated reflections were reduced to 956 independent reflections) to $(\sin\theta/\lambda)_{max} = 0.88$ Å^{-1} and an accurate empirical absorption correction ($\mu_l = 25.14$ mm^{-1}) was carried out based on the very large redundancy of the data set (SADABS). The structure solution and refinement was done with SHELXL (ref. 24).

SINGLE-CRYSTAL STRUCTURE REFINEMENT

The final structure refinements were done using anisotropic displacement parameters on all atoms (Table 3), using restraints. The final interstitial model for the single-crystal data restrains the anisotropic displacement parameters of the Zn interstitials to approximate isotropic behaviour (ISOR 0.1 command[24]). This keeps the thermal ellipsoids from extending into the neighbouring Zn(1) or Zn-interstitial positions. In addition, the total Zn stoichiometry was restrained to the Zintl stoichiometry ($x = 3.9$, with standard deviation 0.36) for a final stoichiometry $x = 3.83(4)$. In this way both the occupancy and anisotropic thermal parameters are allowed to vary within physically reasonable restraints.

The reliability factor R_F is defined as

$$R_F = \frac{\Sigma\left|\,|F_o| - |F_c|\,\right|}{\Sigma|F_o|}$$

where F_o and F_c are the observed and calculated structure factors. Goodness-of-fit (GooF) is defined as

$$\mathrm{GooF} = \sqrt{\frac{\Sigma w(F_o^2 - F_c^2)^2}{N-P}}$$

where N is the number of reflections, P is the total number of parameters refined and w is the weighting function given in the Supplementary Information (Table S1).

Further refinement of the structure is possible (GooF > 1.1) by modelling some of the 1 e Å^{-3} difference peaks as additional Zn-interstitial sites. These additional sites were excluded in the final model because they appear only as non-ellipsoidal bulges in the MEM electron-density map, and therefore their significance is uncertain.

POWDER SAMPLE PREPARATION AND X-RAY DIFFRACTION

The powder sample was obtained by direct reaction of the constituent elements. Room-temperature synchrotron powder-diffraction measurements were carried out at the beam line BL02B2 at SPring8, Japan, using a large Debye-Sherrer camera with an image plate detector[25]. The incident X-ray wavelength ($\lambda = 0.42061$ Å) was determined by calibration on a standard CeO_2 sample ($a = 5.411102$ Å). The image plates were scanned with a pixel resolution of 100 μm. The data extend from $2\theta = 3°$ to $2\theta = 39°$ with a step size of 0.01° ($d_{min} = 0.626$ Å).

RIETVELD AND MEM

Owing to the small diameter of the capillary (0.1 mm) and the high energy of the incoming X-rays, absorption and extinction are negligible. In addition, powder-diffraction data cannot contain spurious effects from twinning. This makes the synchrotron data more suitable for MEM calculations than the single-crystal data, as is confirmed by the smooth MEM densities with very little noise. In combined Rietveld/MEM analysis[26], a small impurity phase of metallic Zn is also observed. As a starting point we Rietveld-refined a model without interstitial Zn atoms. From this refinement, structure factors were extracted for MEM calculations, and the corresponding density revealed several positions of interstitial atoms. The largest interstitial peak was included in the Rietveld model and the procedure was repeated. In the following two Rietveld/MEM cycles, a total of three interstitial sites were added to the model. Final residual values for the refinement with the three zinc interstitial sites (refined stoichiometry $Zn_{3.845}Sb_3$) were $R_P = 2.03\%$, $R_{WP} = 2.68\%$, $R_F = 2.37\%$ (for 802 reflections with $d_{min} = 0.626$ Å).

The reliability factor RP is defined as

$$R_P = \frac{\Sigma|Y_o - Y_c|}{\Sigma|Y_o|}$$

where Y_o and Y_c are the observed and calculated intensity. R_{WP} is the reliablity factor based on the weighted powder profile:

$$R_{WP} = \sqrt{\frac{\Sigma w(Y_o - Y_c)^2}{\Sigma w Y_o^2}}$$

and $w = 1/Y_o$ is the weighting function.

It should be stressed that MEM analysis on the single-crystal data produce approximately the same three interstitial Zn sites as does the MEM analysis of the synchrotron powder data. However, for the single-crystal analysis the interstitials are superimposed on a more noisy background density. MEM calculations use scaled, phased, 'error free' (that is, corrected for systematic errors such as extinction and absorption) structure factors as input for finding the numerical grid density (ρ_x) that optimizes $S = -\rho_x \log(\rho_x/\tau_x)$ subject to the constraints of the data,

$$\chi^2 = \frac{1}{N}\Sigma\left(\frac{F_{obs} - F_{model}}{\sigma(F_{obs})}\right)^2 = 1 \quad .$$

Here S is the Shannon entropy, τ is the grid density derived from prior information, N is the number of the observed structure factors, and σ is the standard deviation.

The ENIGMA program[9] was used for parallel code MEM calculations at the Danish Supercomputer Centre. The calculations used uniform priors and a 240 × 240 × 240 pixel grid. Iterations were stopped at $\chi^2 = 1$ with $R_F(\mathrm{MEM}) = 2.15\%$.

Received 4 January 2004; accepted 20 April 2004; published 27 June 2004.

References

1. Caillat, T., Fleurial, J. P. & Borshchevsky, A. Preparation and thermoelectric properties of semiconducting Zn_4Sb_3. *J. Phys. Chem. Solids* **58,** 1119–1125 (1997).
2. Skrabek, E. A. & Trimmer, D. S. in *Thermoelectric Handbook* (ed. Rowe, D. M.) 267–275 (CRC, Boca Raton, 1995).
3. Uher, C. in *Recent Trends in Thermoelectric Materials Research I* (ed. Tritt, T. M.) 139–253 (Academic Press, San Diego, 2001).
4. Sales, B. C., Mandrus, D. & Williams, R. K. Filled skutterudite antimonides: A new class of thermoelectric materials. *Science* **272,** 1325–1328 (1996).
5. Slack, G. A. in *Thermoelectric Handbook* (ed. Rowe, M.) 407–440 (CRC, Boca Raton, 1995).
6. Sales, B. C. Electron crystals and phonon glasses: a new path to improved thermoelectric materials. *Mater. Res. Soc. Bull.* **23,** 15–21 (1998).
7. Mayer, H. W., Mikhail, I. & Schubert, K. Phases of $ZnSb_N$ and $CdSb_N$ mixtures. *J. Less-Common Metals* **59,** 43–52 (1978).
8. Caillat, T., Borshchevsky, A. & Fleurial, J.-P. in *Thermoelectric Materials - New Directions and Approaches. Symposium* (eds Tritt, T. M., Kanatzidis, M. G., Lyon, H. B. Jr & Mahan, G. D.) 103–108 (Materials Research Society, San Francisco, California, 1997).
9. Tanaka, H. *et al.* ENIGMA: maximum-entropy method program package for huge systems. *J. Appl. Crystallogr.* **35,** 282–286 (2002).
10. Bokii, G. B. & Klevzova, R. F. X-ray structure investigation of the beta-phase in the zinc-antimony system. *Zh. Strukt. Khim.* **6,** 866 (English-translated pages 830–834) (1965).
11. Izard, V., Record, M. C., Tedenac, J. C. & Fries, S. G. Discussion on the stability of the antimony-zinc binary phases. *CALPHAD* **25,** 567–581 (2001).
12. Kim, S. G., Mazin, II & Singh, D. J. First-principles study of Zn-Sb thermoelectrics. *Phys. Rev. B* **57,** 6199–6203 (1998).
13. Kauzlarich, S. M. (ed.) *Chemistry, Structure, and Bonding of Zintl Phases and Ions* (VCH, New York, 1996).
14. Papoian, G. A. & Hoffmann, R. Hypervalent bonding in one, two, and three dimensions: Extending the Zintl-Klemm concept to nonclassical electron-rich networks. *Angew. Chem. Intl Edn* **39,** 2409–2448 (2000).
15. Rowe, D. M. (ed.) *CRC Handbook of Thermoelectrics* (CRC, Boca Raton, 1995).
16. Chung, D. Y. *et al.* $CsBi_4Te_6$: A high-performance thermoelectric material for low-temperature applications. *Science* **287,** 1024–1027 (2000).
17. Miller, R. C. in *Thermoelectricity: Science and Engineering* (eds. Heikes, R. R. & Ure, R. W.) 405–407 (Interscience, New York, 1961).
18. Funke, K. in *Superionic Solids and Solid Electrolytes Recent Trends* (eds Laskar, A. L. & Chandra, S.) 569–629 (Academic, San Diego, 1989).
19. Souma, T., Nakamoto, G. & Kurisu, M. Low-temperature thermoelectric properties of alpha- and beta- Zn_4Sb_3 bulk crystals prepared by a gradient freeze method and a spark plasma sintering method. *J. Alloy. Comp.* **340,** 275–280 (2002).
20. Shaver, P. J. & Blair, J. Thermal and electronic transport properties of *p*-Type ZnSb. *Phys. Rev.* **141,** 649–663 (1966).
21. Yvon, K., Baillif, R. & Flukiger, R. Positional disorder and nonstoichiometry in $Cu_{2-X}Mo_3S_4$ compounds 2: Triclinic low-temperature structure of $Cu_{2-X}Mo_3S_4$. *Acta Crystallogr. B* **35,** 2859–2863 (1979).
22. Caillat, T., Fleurial, J.-P. & Snyder, G. J. Potential of Chevrel phases for thermoelectric applications. *Solid State Sci.* **1,** 535–544 (1999).
23. Cahill, D. G., Watson, S. K. & Pohl, R. O. Lower limit to thermal conductivity of disordered crystals. *Phys. Rev. B* **46,** 6131–6140 (1992).
24. Sheldrick, G. M. *SHELXL-97 A Program for Crystal Structure Refinement* (Univ. Göttingen, Germany, 1997).
25. Nishibori, E. *et al.* The large Debye-Scherrer camera installed at SPring-8 BL02B2 for charge density studies. *Nucl. Instrum. Methods A* **467,** 1045–1048 (2001).
26. Takata, M., Nishibori, E. & Sakata, M. Charge density studies utilizing powder diffraction and MEM. Exploring of high T_c superconductors, C-60 superconductors and manganites. *Z. Kristall.* **216,** 71–86 (2001).

Acknowledgements

We would like to thank Philippe Rabiller, Sossina Haile, Franck Gascoin and Peter Stephens for discussions and preliminary results, and Helena Kauppila for Ga-doping experiments. The Danish Research Councils are acknowledged for funding through the DANSYNC centre, and access to a 512-node PC cluster at the Danish Supercomputer Centre, Southern Denmark University. E. N. thanks M. Sakata and M. Takata for valuable discussions, and K. Kato for experimental help at SPring-8. The synchrotron radiation experiments were performed at beam line BL02B2 at SPring-8 with the approval of the Japan Synchrotron Radiation Research Institute (JASRI). We also thank the European Commission for financial support under the NANOTHERMEL contract. This work was supported in part by the National Science Foundation Center for the Science and Engineering of Materials at Caltech and the Defence Advanced Research Projects Agency at the Jet Propulsion Laboratory under contract with NASA.

Correspondence and requests for materials should be addressed to G.J.S.

Supplementary Information accompanies the paper on www.nature.com/naturematerials

Competing financial interests

The authors declare that they have no competing financial interests.